The use of passive baffles to increase the yield of a single slope solar still

D.E. Benhadji Serradj, T.N. Anderson* and R.J. Nates

Department of Mechanical Engineering, Auckland University of Technology, New Zealand

Abstract

Despite their relative simplicity, single slope solar stills remain one of the most viable solutions to the production of freshwater from saline and non-potable water sources. Over the years, numerous researchers have attempted to improve the yield of single slope solar stills through changes to their geometry and the use of various design modifications. Despite this long history of research, one modification that has not been fully explored is the use of passive baffles to alter the natural convection inside them.

Though baffles have frequently been used to suppress natural convection in enclosures, there may also be the opportunity to use them to enhance natural convection. This judicious placement of baffles to enhance the natural convection could potentially improve the yield from single slope solar stills, however it has not been well explored in the literature.

To address this issue, this work examined the effect of vertically mounted passive baffles on the natural convection inside a single slope solar still geometry. In this vein, a computational fluid dynamics simulation was conducted for a still containing a baffle, with the results validated experimentally using particle image velocimetry. On this basis, subsequent simulations explored the effect of baffle length and position on stills with cover angles from 10˚-60˚. The results showed that baffles did have a marked influence on the natural convection flow field and could increase the natural convection heat transfer coefficient, which is directly proportional to a solar still's yield, by up to 20%.

It was also found that short baffles enhanced natural convection at low cover angles, while baffles mounted close to the front of a still provided an improvement to the transfer processes over the widest range of conditions. Finally, the work led to the development of a relationship to describe the effect of baffles on natural convection, as shown in Equation 1, that it is hoped will aid designers of single slope solar stills in the future.

*Corresponding author: timothy.anderson@aut.ac.nz

$$Nu' = Ra'^{0.188} * AR^{-0.29} * (\cos\theta)^{-0.5} * \left(\frac{b}{B}\right)^{0.08} * \left(\frac{d}{D}\right)^{0.09} \quad (1)$$

Keywords: *Natural convection; single slope solar still; heat and mass transfer*

Nomenclature

Latin symbols

AR	Aspect ratio (B/L)
b:	Baffle position
B	Base
C_p:	Specific heat
d:	Baffle height
D:	Total height at baffle position
g:	Gravity
h:	Heat transfer coefficient
k:	Thermal conductivity of humid air
L:	Characteristic length (average enclosure height)
M:	Molar weight of air and water vapour mixture
Nu:	Nusselt number
Nu':	Modified Nusselt number
P:	Pressure
r:	Radius
Ra:	Rayleigh number
Ra':	Modified Rayleigh number
T:	Temperature
u:	X-component of velocity
v:	Y-component of velocity
W:	Width
ΔT:	Temperature difference between water and glass
Δt:	Time difference
ΔT':	Modified temperature difference between water and glass
X:	X component
Y:	Y component

Subscripts

a:	Humid air
c:	Cold surface (Glass cover)
cv:	Convective
ew:	Evaporative
h:	Hot surface (Water surface)
p:	Polyamide particles
s:	Silicon oil
t:	Total

Greek symbols

μ:	Viscosity
λ:	Thermal conductivity
β:	Volume expansion coefficient

φ: Heat flux
ρ: Density
τ_s: Relaxation time
θ: Inclination angle

1. Introduction

Although earth is called the blue planet, world water resources are under extreme stress. Over 1-billion people live in regions where water is scarce and are unable to afford fresh water for their daily basic needs. Because of this, goal six of the United Nations' Agenda 2030 considers water accessibility as paramount to reaching its sustainable development goals (Gude, 2017, Hák et al, 2016). As a result of freshwater resources depletion, numerous methods have been developed to generate fresh water from non-potable sources. However, most of these technologies, such as reverse-osmosis systems, are implemented where abundant conventional energy resources are available. Furthermore, such technologies often require large amounts of energy to operate and face economic challenges when being scaled down. This makes solar distillation one of the most practical solutions to the production of fresh water particularly in regions endowed with high solar energy potential.

Despite the recent developments in solar distillation systems, such as the inclusion of thermal collectors and photovoltaic systems (active solar distillation) (Tiwari et al, 2020, Gaur and Tiwari, 2010, Mediouli et al, 2020, Kumar et al, 2010), passive solar distillation systems still remain attractive due to their low cost, easy maintenance and reliance on solar energy only. This makes them a promising option for water distillation in remote areas (Parsa et al, 2020, Kumar and Tiwari, 2009, Tiwari and Sahota, 2017). Furthermore, of all the passive solar still configurations, the single slope (SS) solar still is perhaps the simplest, and frequently serves as a benchmark to which other techniques are compared (Velmurugan et al, 2008).

To briefly outline, a passive single slope solar still operates on the principle of evaporation and condensation of water. The still takes the form of a trapezoidal cavity composed of two main parts: an absorber basin (often a black painted surface) and a transparent glass cover. The incident solar radiation is transmitted through the glass cover and absorbed by the black absorber basin, where the non-potable water is held. With the rising temperature of water in the basin, convective and evaporative heat transfer carry water vapor from the basin to the glass cover, where it condenses as fresh water and is collected.

Over the years extensive research has been carried out in an attempt to enhance the productivity of these devices. Several inventive methods, such as utilizing different absorber materials (Arunkumar et al, 2018, Panchal et al, 2017), including thermal energy storage (Yousef and Hasan, 2019, Sakthivel and Arjunan, 2019), varying the cover tilt angle (Cherraye et al 2020. Azooz and Younis, 2016, Dev and Tiwari, 2009), adding external condensers (Hassan et al 2020, Al-Hamadani and Shukla, 2013), adding features to increase the absorption area El-Sabaii and El-Naggar, 2017, El-Sabaii et al, 2015), using fins within the enclosure (Subhani and Kumar, 2019, El-Sabaii et al, 2000) and using mirrors to increase the incident radiation (Karimi Estahbanati et al, 2016, Tanaka, 2009) have all been examined. Given this extensive body of literature, the area has also been the subject of research reviews describing the different parameters that influence the performance of single slope solar stills (Pachal and Patel, 2017, Sharshir et al, 2016).

Now reflecting on the operation of a single slope solar still, it is apparent that the principle transport mechanism is through natural convection, hence most researchers use the Chilton-Colburn analogy (Abdallah et al, 2009) to determine the ratio between convective heat transfer and evaporation rates. Knowing that evaporation rate is directly proportional to the convective heat transfer, increasing the later parameters leads to a direct increase in single slope solar still performance. In this vein, numerous researchers have experimentally investigated the effect of natural convection on evaporative heat transfer and subsequently water yield. Kumar and Tiwari, (1996) experimentally examined the convective mass transfer in solar distillations systems and concluded that accuracy in the estimation of convective heat transfer coefficient is paramount to the prediction of the performance of single slope solar stills. More recently, Tiwari and Tiwari, (2005) reported that for a constant temperature difference between the water and glass cover, a small variation in the convective heat transfer coefficient results in a significant variation in the evaporative heat transfer coefficient. Dwivedi and Tiwari, (2009) compared internal heat transfer coefficients experimentally and found that the convective heat transfer coefficient directly affected the evaporative heat transfer coefficient and thus water yield. Similarly, Sampathkumar et al. (2010) found that the evaporative heat transfer was strongly dependent on natural convective heat transfer.

Given these findings, several researchers have attempted to increase the performance of single slope solar stills by exploring the effect of different geometrical parameters. Recently, Keshktar et al. (2020) investigated the effect of the angle and aspect ratio on the performance of single

slope solar stills using transient CFD modelling. The results of the study suggested that at a 30º cover angle, a low aspect ratio reduced productivity because of the water basin being close to the glass cover (ambient conditions).

Feilizadeh et al. (2017) presented an optimization study of a single slope solar still performance by varying the aspect ratio, cover angle and the geometry width. It was found that decreasing the aspect ratio decreased the solar still performance. However, it was found that the length was proportional to the productivity and increasing solar still width was found to increase the performance to an optimum beyond which the performance decreased. That said, it is worth mentioning that the previous results were based on Dunkle's correlation, which despite its widespread use is a poor representation of a single slope solar still.

Jamil and Akhtar (2017) investigated experimentally the effect of varying the aspect ratio on the productivity of a single slope solar still. They concluded that increasing the aspect ratio increases the performance of the solar still, which is the opposite to what has been reported by Keshktar et al. (2020). The authors believe that the increase in performance is due to the short distance between the water basin and cover glass leading to a faster heat exchange between the two boundary layers.

An experimental investigation was performed by Azooz and Younis (2016) to identify the effect of the cover angle and aspect ratio on the performance of a single slope solar still. It was found that a solar still with a cover angle equal to 35º (latitude of the location) and an aspect ratio 1.8 produces less water than a single slope solar still with a 25º cover angle and aspect ratio 2.4. Furthermore, high cover angle high aspect ratio geometries were found to produce more water than solar stills with cover angle equal to the latitude 35º. However, they are less advantageous than lower angle solar stills when looking at the economic feasibility of such devices. As such these findings contradict the conclusion made by Jamil and Akhtar (2017) and Keshktar et al. (2020) related to the selection of the best cover angle and aspect ratio. These contradictions raise several interesting questions about the performance of single slope solar stills.

In an alternate vein, El-Sebaii and Naggar (2015) experimentally investigated the effect of using fins in the absorber basin in an attempt to increase natural convection heat transfer in the water. The results of the experiment showed an improvement of approximately 17% compared to a conventional single slope solar still, though varying fin material did not significantly affect

the overall performance. Along a similar line, Sebaii et al. (2000) attempted to increase the yield of a single slope solar still using a horizontally suspended baffle absorber. The authors reported an increase of 18% in efficiency compared to a conventional solar still with the optimum configuration being in the middle of the basin. Similarly, a solar still with extended porous fins from the absorber was experimentally investigated by Srivastava and Agrawal (2013). Results of their study have showed a faster and early morning start-up resulting in a higher performance compared to conventional configuration. However, it is likely that these performance improvements can be attributed to the creation of a thinner film of water being created in the basin.

An alternative use of baffles would be to alter the air flow between water surface and the glass cover, potentially enhancing the natural convection in the solar still. Moukalled and Darwish (2000) computationally examined the natural convection in a trapezoidal enclosure with a cover angle of 15º and baffles mounted on the inclined surfaces, as an analogy of an attic space. In their study two conditions were investigated: summerlike and winterlike conditions. During the winter season (where the boundary conditions are similar to a single slope solar still's working conditions) it was found that, for a given baffle length, heat transfer increases with an increasing distance from the lower side wall.

Similarly, Varol et al. (2007) numerically investigated the effect of a thin fin on the natural convection inside a triangular enclosure. Their results showed that including fins on the bottom wall modified the rotational direction of vortices in the enclosure. Furthermore, the Nusselt number was found to increase with the increase of Rayleigh number but remained relatively constant at low Rayleigh numbers due to the dominance of conductive heat transfer, and it was concluded that increasing the length of the fin inside the cavity blocked the flow and reduced the heat transfer coefficient (passive control of fluid flow and heat transfer).

However, Rashidi et al. (2016) numerically and experimentally investigated the effect of vertical baffle attached to the absorber on the single slope solar still performance. In their study, a solar still with a baffle positioned at the midpoint of the absorber and a cover angle of 12.5º was considered. Their results have showed that the use of the baffle increased the performance of the solar still by almost 8% compared to the conventional configuration. Furthermore, the increase in performance was due to the creation of additional cells in the geometry. In another study, Rashidi et al. (2016) performed an optimization study to determine the baffle configuration that leads to the highest single slope solar still performance. The investigation

was conducted on a solar still with an angle of 14.5º and temperature difference between the absorber and cover of 15º C. The results of the study showed that the length of the baffle and position directly affect the heat transfer inside the cavity by creating additional vortices, thus increasing solar still performance. Furthermore, the location and length of the baffle depends on whether the baffle is mounted on the absorber or cover surface.

In a recent attempt, Subhani and Kumar (2019) numerically investigated the effect of baffles on the performance of a single slope solar still with a fixed cover angle. The study found that in some cases, mounting a baffle supresses natural convection inside the geometry which leads to a deterioration of the fluid flow resulting in a lower heat transfer coefficient. Moreover, the author concluded that the best location was 1/2 of the absorber distance which contradicts the findings reported by Rashidi et al. (2016).

With reference to the literature, it is apparent that numerous researchers have shown great interest in the enhancement of single slope solar stills by varying their geometry, and a few have investigated the effect of mounting baffles on their performance. Having said that, the effect of baffles has not been studied in a generalizable way and there appear to be several contradictory findings in the work that has been performed. Therefore, the purpose of this study is to fill the gap presented by the previous work by investigating, in detail, the influence of vertical baffles on the natural convection inside a single slope solar still geometry. In doing this it aims to define the relationship between the baffle length, its position in the still and the other geometric parameters that will aid in predicting the performance of single slope solar stills.

2. Method

To ascertain the effect of baffles in a solar still enclosure, a numerical investigation of natural convection inside a solar still-like geometry was performed using ANSYS's commercial computational fluid dynamics (CFD) software, FLUENT 20.2. CFD has demonstrated its abilities in undertaking reliable analysis and has been extensively applied to the analysis of natural convection inside enclosures, as experiments to independently study molecular diffusion and buoyant convection are complex and expensive (Rahbar and Esfahani, 2012). That said, many researchers have shown CFD and obtain results in good agreement with the experimental work (Djebedjian and Rayan, 2000, Rahbar and Esfahani, 2012, Omri and Orfi, 2005, Rheinlander, 1982)

Due the lower cost of CFD, compared to building real experiments, and the ability to the test extensive range of parameters affecting thermal behaviours inside single slope solar stills, several researchers have attempted to study these geometries with the help of CFD (Siva Sankaran and Sridharan, 2020, Rashidi et al 2018, Panchal and Patel, 2018, Alipanah and Rahbar, 2018). According to Rincón-Casado et al. (2017), investigation of natural convection and flow behaviours in three dimensional enclosures is complex (convergence difficulty) and time consuming. Moreover, several researchers in the field of heat and mass transfer simplified these problems to two dimensional while maintaining good agreement with experimental results. Now broadly speaking single slope solar still geometry does not vary in z direction, and typically stills are long, meaning there are limited effects due to the side walls. Hence, in this study, the flow was taken to be two dimensional.

As shown in Figure 1, the enclosure investigated was a trapezoidal enclosure similar to a single slope solar still geometry, with a thin baffle attached to the top surface. In constructing the geometry, the base was taken to have a unit length, and the front wall a height of one-tenth of this. The bottom and the top inclined surfaces were differentially heated, and the side walls were assumed to be adiabatic (as was the baffle), since in solar still side walls are well insulated to reduce heat loss.

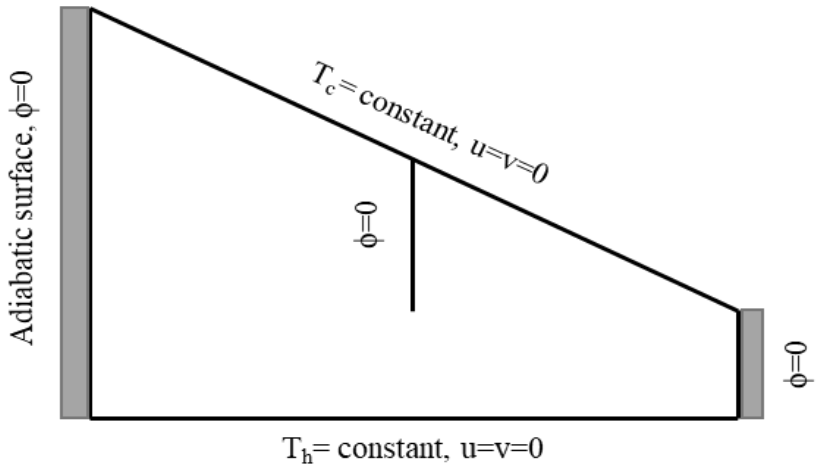

Figure 1: Imposed boundary conditions.

Finally, the cover was varied over a range of angles which led to changes in mean enclosure height, this in turn led to the enclosure being modelled at several aspect ratios as shown in Table 1.

Table 1: CFD geometry configurations

Cover angle (θ)	Aspect ratio (AR)
10˚	5.31
20˚	3.55
30˚	2.57
40˚	1.92
50˚	1.44
60˚	1.04

In modelling the flow, it was assumed that the cavity would be filled with humid air in order to reproduce the same physical phenomena observed between the water surface and glass cover in solar stills. By varying the temperature differential between the base and the cover, Rayleigh numbers between 3.37×10^{6} and 3.03×10^{9} were examined.

Given the range of Rayleigh numbers, it was necessary to consider the treatment of turbulence within the enclosure. Flack (1980) experimentally investigated fluid flow inside double slope trapezoidal enclosures and found out that the transition from laminar to turbulent flow occurs at $Ra = 0.7\times10^{5}$. Poulikakos and Bejan (1983) also performed experimental flow visualization of air inside a trapezoidal shape and found that the flow was turbulent at $Ra = 4.7\times10^{8}$. Given these findings, and because the range of Rayleigh number range in this study fall between 3.37×10^{6} and 3.03×10^{9}, the current study considered the flow to be turbulent. As such, the turbulence field was resolved using the Realizable k-ε model, which has proven to be suitable for simulating natural convection inside cavities and flow near the walls (Rincón-Casado et al, 2017, Altaç and Uğurlubilek, 2016).

In resolving the discretized form of the continuity equations, the pressure-velocity coupling was handled using a coupled algorithm, as it offers a robust and efficient solution for steady state flows. The convection-diffusion terms were solved using a second order upwind approach, for higher accuracy (ANSYS Inc, 2015) and since the temperature changes in the working fluid were small, the Boussinesq approximation was applied in the treatment of the buoyancy. In solving the continuity equations, the solution was considered to be fully converged when the residuals of all equations were lower than 10^{-5}.

Finally, to reduce simulation time without decreasing the accuracy of CFD results, it was necessary to perform a grid sensitivity analysis. In this study, the heat transfer coefficient

(determined by the simulation) on the bottom hot surface was compared for different element sizes, leading to different numbers of mesh elements. In this way, a better convergence of heat transfer coefficient can be achieved leading to an independent solution from the computational grid. Since the geometry varies in the current numerical study, it was decided to perform the mesh sensitivity for two enclosures with different cover angles, 10º and 40º with a fixed baffle length (5/6) and position (2/3). Figure 2 shows the variation of heat transfer coefficient from the bottom surface for different angles and element sizes. Based on the results, a 10^{-3} m element size was selected because of the relatively small change in the heat transfer coefficient after a 3 x 10^{-3} m element size.

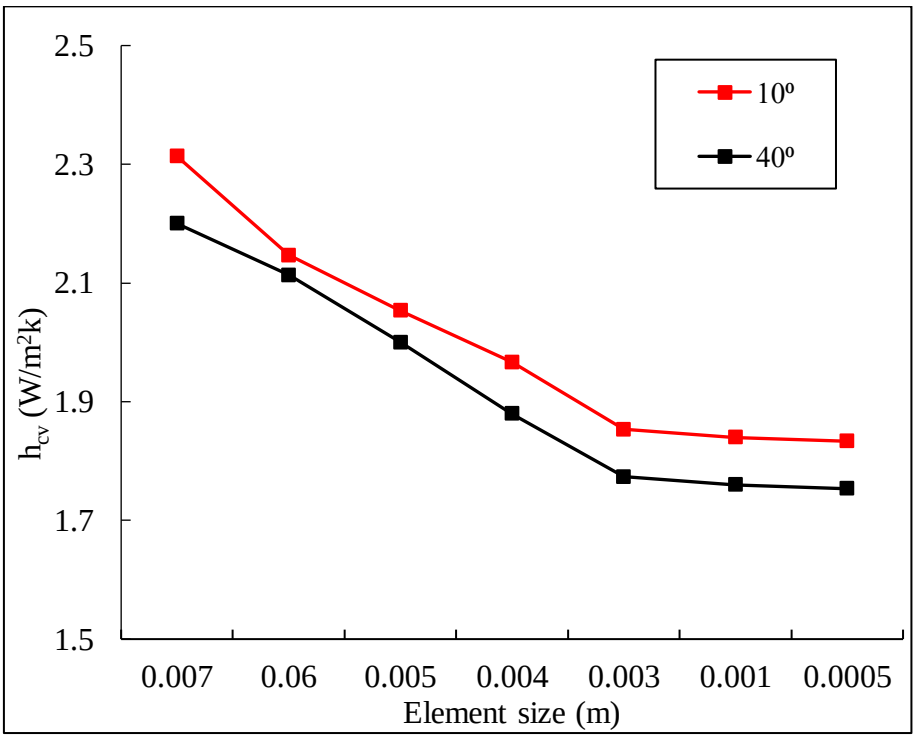

Figure 2: Variation of heat transfer coefficient with the element size at (ΔT=15ºC).

3. Validation

Before proceeding to a full CFD analysis however, it was necessary to validate the selected numerical model. To achieve this, it was decided to undertake a particle image velocimetry (PIV) study of the flow in a typical still geometry fitted with a baffle. In this vein an experimental enclosure 0.4 m x 0.4 m (B x W) was fabricated, with front wall and back wall heights of 0.1 m and 0.331 m respectively giving a cover inclination (θ) of 30º and aspect ratio

(AR) of 1.86. Furthermore, a baffle with a length (d) of 0.16 m was fixed 0.13 m (~1/3 of the base) from the front wall (b=0.13 m), as shown in Figure 3.

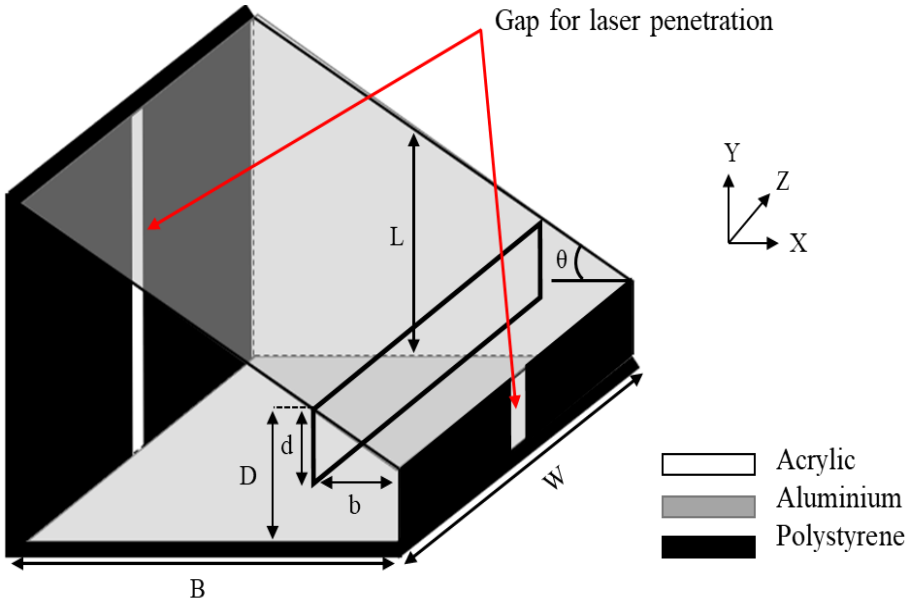

Figure 3: Experimental enclosure.

Now, under the normal working conditions of solar stills, saturated air transports water vapor from the basin to the cover. However, since the aim of the study was to investigate natural convection inside a single slope solar still-like enclosure with a vertical baffle, silicon oil (100cSt) was used as an analogue to the air vapour as this better facilitated the seeding of particles in the flow. As such, the working fluid (silicon oil) and experimental geometry properties were chosen to match the Rayleigh numbers (Equation 2) typically encountered in single slope solar stills.

$$Ra_s = \frac{\rho_s{}^2 \, g \, \beta_s \, (T_h - T_s) \, Cp_s \, L^3}{\lambda_s \mu_s} \qquad (2)$$

To replicate the absorption of solar radiation in the basin, an adhesive electrical heating element of 120W was attached to a 3 mm thick aluminium sheet to form the base of the enclosure. Aluminium was used in order to achieve a uniform temperature on the surface and avoid bending due to the mass of the silicon oil. To avoid heat losses from the bottom surface, 40 mm expanded polystyrene foam (EPS) sheet was used to insulate the heater from the ambient environment and maximise the heat going into the generation of the natural convection.

Since the cover in a solar still has a lower temperature than the absorber it was necessary to replicate this scenario. In this respect, another 3 mm aluminium sheet was used as the cover, as noted previously this allowed a uniform temperature to be maintained while providing mechanical strength. An electric fan was used to circulate cool ambient air (~3 m/s) over this surface to maintain a temperature difference between the 'absorber' and 'cover'. As such, the experimental design was like that used by Anderson et al (2010) in their study of natural convection in a triangular enclosure.

To allow the penetration of the laser sheet used in the PIV system, and to visualise the flow inside the geometry the back, front, baffle and side walls were made of 10 mm clear acrylic sheets. As with the heater, the front and back walls were insulated using 40 mm EPS foam sheets to reduce heat loss. However, the side walls could not be insulated as optical access for the camera was required.

In addition, 16 Copper-Constantan (T-type) thermocouples were used to monitor the temperature difference between the absorber and cover. Each surface (bottom and top) had seven thermocouples attached to it, with the remaining two used to measure the room temperature, with results recorded using a Picolog TC-08 multi-channel data logger. These measurements were used to identify steady state flow conditions which could be used for the PIV. Typically, this occurred at least 10 hours after start-up, as shown in Figure 4.

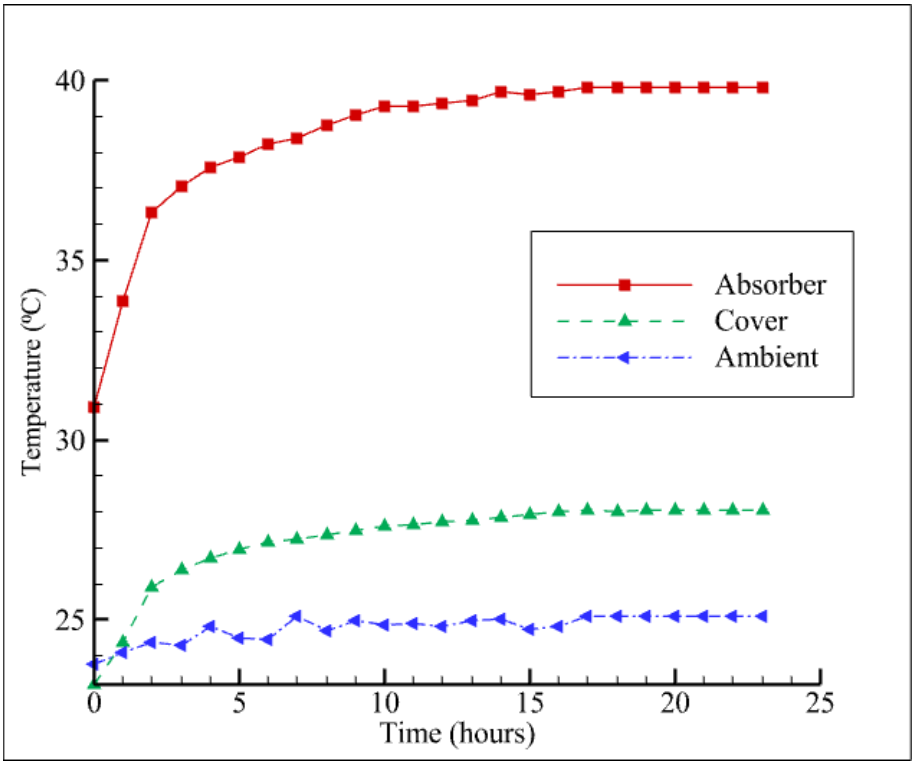

Figure 4: Experimental steady-state temperature measurement.

In performing the PIV measurements, a Microvec PIV system (Figure 5) was used to visualize the flow features inside the cavity. The system was composed of a charge-coupled device (CCD) camera and a dual-pulse PIV laser, synchronised using a MicroPulse725 synchronizer. To track the fluid flow inside the cavity, round polyamide particles with 50 µm diameter were used due to their low relaxation time (Equation 3) and gravitational induced velocity (Equation 4) making them neutrally buoyant in silicone oil. Since the cross-section area of the geometry was wider than the camera viewing area (frame), it was necessary to divide the PIV measurement to seven subareas to cover the enclosure height and width. This mirrors the approach used previously by Lartigue et al (2000) and Wu et al (2019).

Once thermal steady state conditions were achieved, 800 pairs of images were acquired for each sub-area in a time interval of Δt=15 ms. Pairs of images (2456 x 2048 pixels) were captured at a pulse delay of 40ms and rate of 16 frames per second by the camera. The images were subsequently processed using the PIVLab package integrated in MATLAB. More details on the PIV technique in general can be found in Raffel et al (2018).

$$\tau_s = (2r_p)^2 \frac{\rho_p}{18\mu_s} \quad (3)$$

$$U_g = d_p^2 \frac{(\rho_p - \rho_s)}{18\mu} g \quad (4)$$

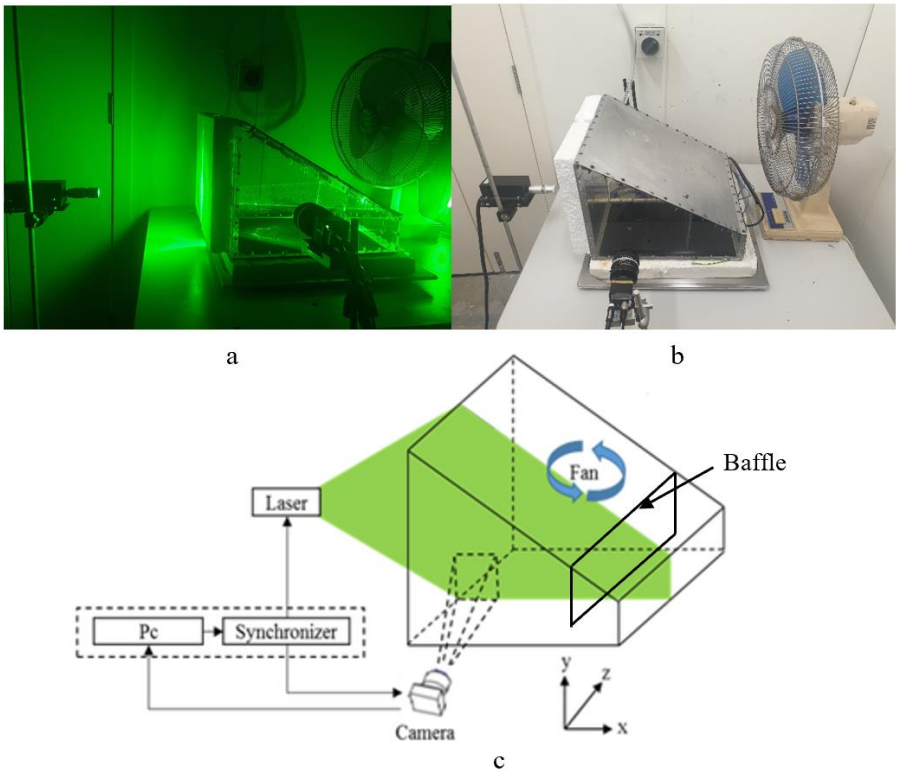

Figure 5: (a) Experimental set up; (b) Laser imaging; and (c) Experimental schematic.

Subsequently, the steady-state boundary conditions acquired from the PIV experiment were applied in a CFD simulation with the same geometry and fluid properties. Figure 6 shows velocity contour at a plane 0.2 m along the geometry length (i.e., in the z-direction).

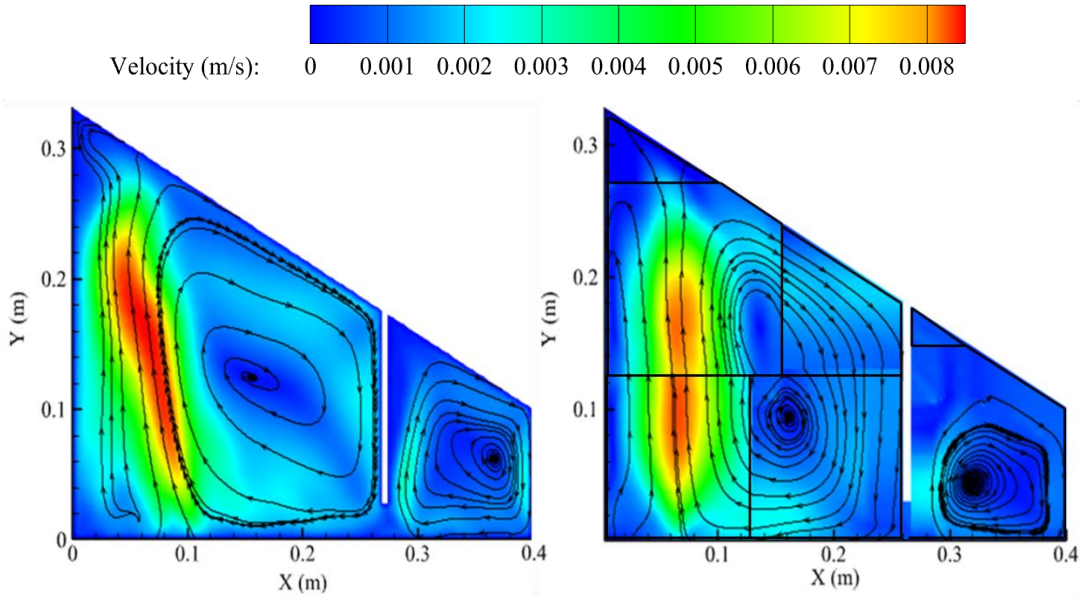

a: CFD b: Experiment

Figure 6: Cross-sectional velocity contours in the middle of the geometry (0.2m, AR=2.6, θ=30º, Ra=1.38×10^{8}), a: CFD simulation, b: experiment.

From the PIV and CFD the same flow features can be seen in the velocity contours and streamlines. In both cases two clockwise rotating cells can be seen (generated by the cooling on the sloped surface), along with a significant plume rising near X=0.8 m. At X=0.27 m, the flow on the left side of the enclosure is forced downwards, toward the hot surface due to the attached baffle, this also facilitates the formation of a secondary cell on right side of the baffle. In addition, a small weak vortex can be noticed under the baffle (in the velocity contours) due to the counter-rotation of the two cells.

As further validation of the method, Figure 7 shows the velocity profile at Y=0.05 m for both the PIV experiment and CFD simulation. In both cases, the velocity magnitude is very low near the left wall. Further from the wall however, the plumes in the contours are translated into velocity peaks reaching $6.9 \times 10^{-3}\, m/s$ in the experiment and $7.5 \times 10^{-3}\, m/s$ in the CFD results. Moreover, as the flow approaches the baffle, a drop in velocity can be seen at X=0.27. Moving past the baffle, another rising plume translated to a relatively high velocity peak at approximatively 0.28 m due to the second recirculation. Furthermore, the velocity drops through the centre of the cell and again increases near the front wall confirming the existence of the secondary cell.

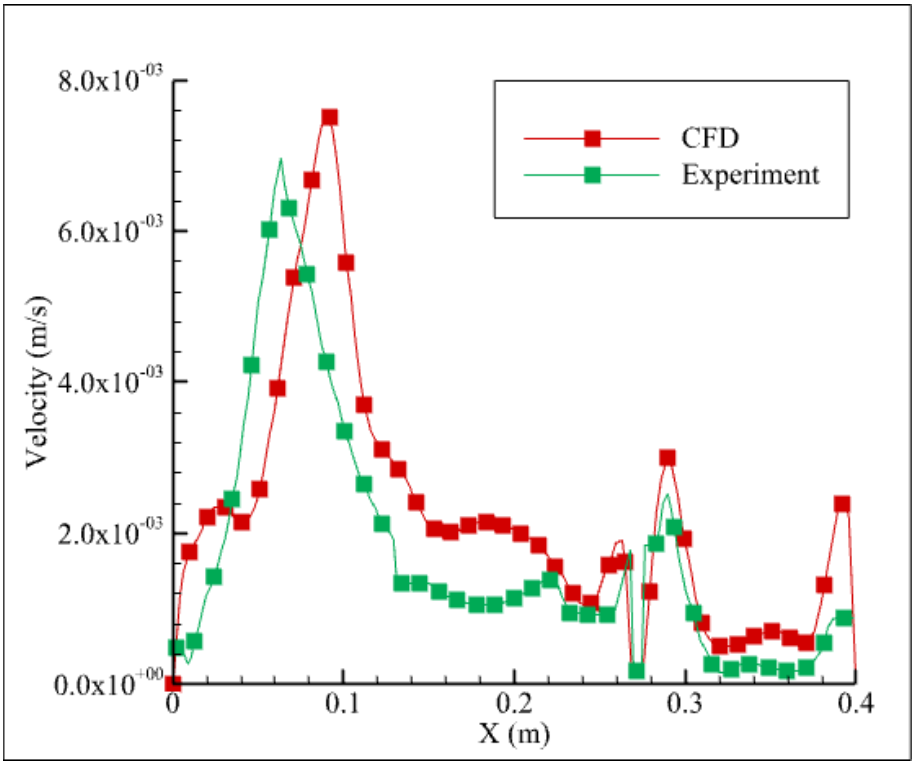

Figure 7: Velocity profile at Y=0.05 m.

Now, it may be argued that the flow in Figure 6 is three dimensional in nature, however this flow is extremely weak, and is an artefact of the small scale and presence of the side walls of the experimental enclosure. In practical solar stills the geometry is better represented as a two-dimensional enclosure, as modelled.

4. Results and discussion

Having validated the numerical scheme, it was decided the investigate the effect of the baffle length and its location on the heat transfer coefficient at the absorber surface for the still. For each cover angle considered, the effect of having a baffle at 1/3, 1/2, 2/3 of the still's width was examined. Furthermore, at each location three baffle lengths:1/6, 3/6, 5/6 of the height (H) between the top and bottom surfaces for the selected baffle position was also studied.

4.1 Baffle mounted near the rear wall of the still

Now as noted previously, the heat transfer coefficient from the absorber surface was determined for a range of cover angles and baffle configurations. Figure 8 shows the effect of

the baffle's length on this when positioned close to the rear wall of the still (1/3 of the still width).

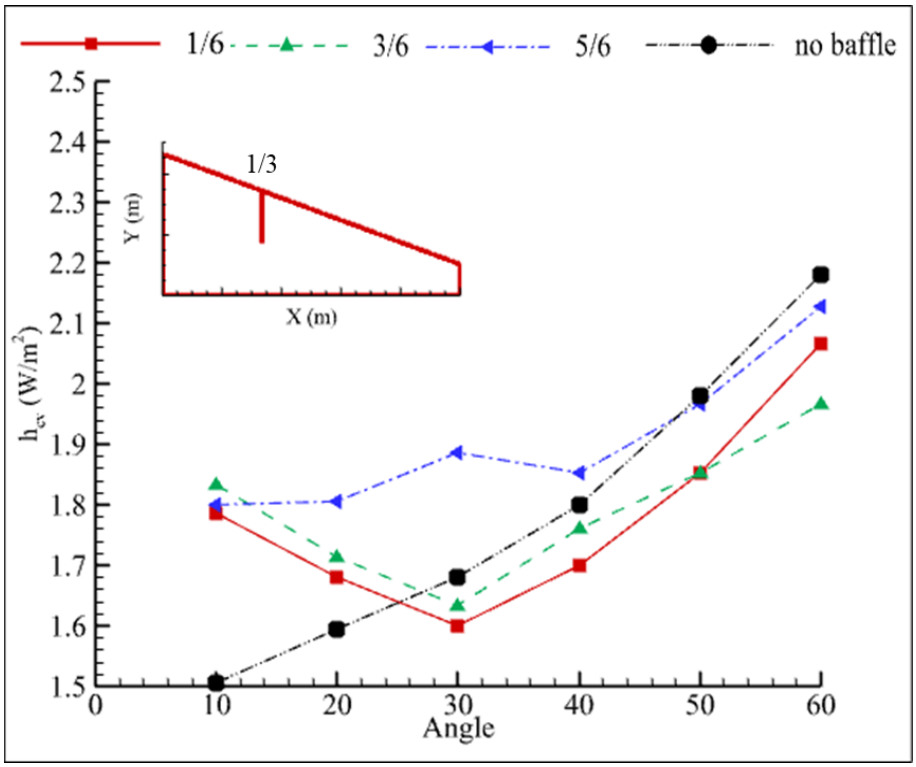

Figure 8: The effect of baffle length and cover angle on the heat transfer coefficient, with the baffle mounted near the rear wall

As is readily apparent, in cases without a baffle, the heat transfer coefficient is proportional to the angle. This can be attributed to the increase in distance between the bottom and top surfaces leading to a velocity increase in the enclosure which leads to a higher heat transfer coefficient, as reported in Asan and Namli (2001). However, what is interesting to note is that at a 10˚ cover angle, having a baffle in the still increases the heat transfer coefficient by approximatively 20%. Now the reasons for this change to the heat transfer coefficient are not readily apparent from Figure 8. However, in Figure 9 it can be seen that the inclusion of a baffle leads to a multi-cellular flow (Bénard-like) pattern being established. For the two shorter baffle lengths (1/6 and 3/6) three cells appear in the flow with areas of relatively high velocity on the absorber surface, thus explaining the increase. For the longest baffle however, the flow generates only two cells, although this still results in an increase in the heat transfer coefficient over the un-baffled case, it represents a decrease from the 3/6 case. In this respect, the baffle has begun to act to suppress rather than enhance convection.

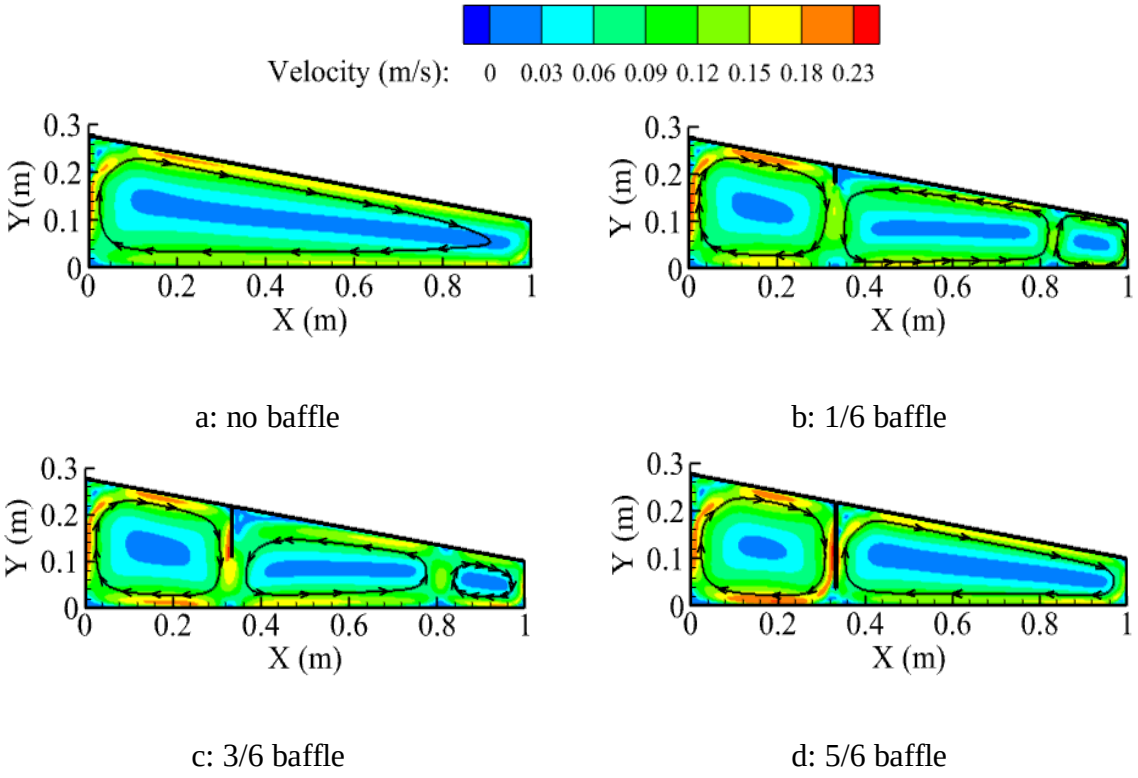

Figure 9: Velocity contours for a cover angle of 10°

Returning to Figure, it is apparent that for a 20° cover angle that the shorter baffles (1/3, 3/6) result in higher heat transfer coefficients than an enclosure without a baffle, though it is somewhat reduced from the preceding example. This implies that the multi-cellular flow is still a feature, though it is having a reduced effect on the heat transfer. To this end, the heat transfer coefficient continues decreasing until it reaches its lowest value at a 30° cover angle, where it is noticeably lower than an enclosure without a baffle. This is a result of a blockage to the flow on the cover surface, caused by the baffle, not allowing the development of the multi-cellular flow structure, and rather, acting to suppress the convection. This is most apparent through the formation of a low velocity recirculation on the lower side of the baffle, as shown in Figure.

Beyond a 30° cover angle, the heat transfer coefficient increases again, however the value of heat transfer coefficient for an enclosure without a baffle is always higher than the geometries with baffles length of 1/6 and 3/6.

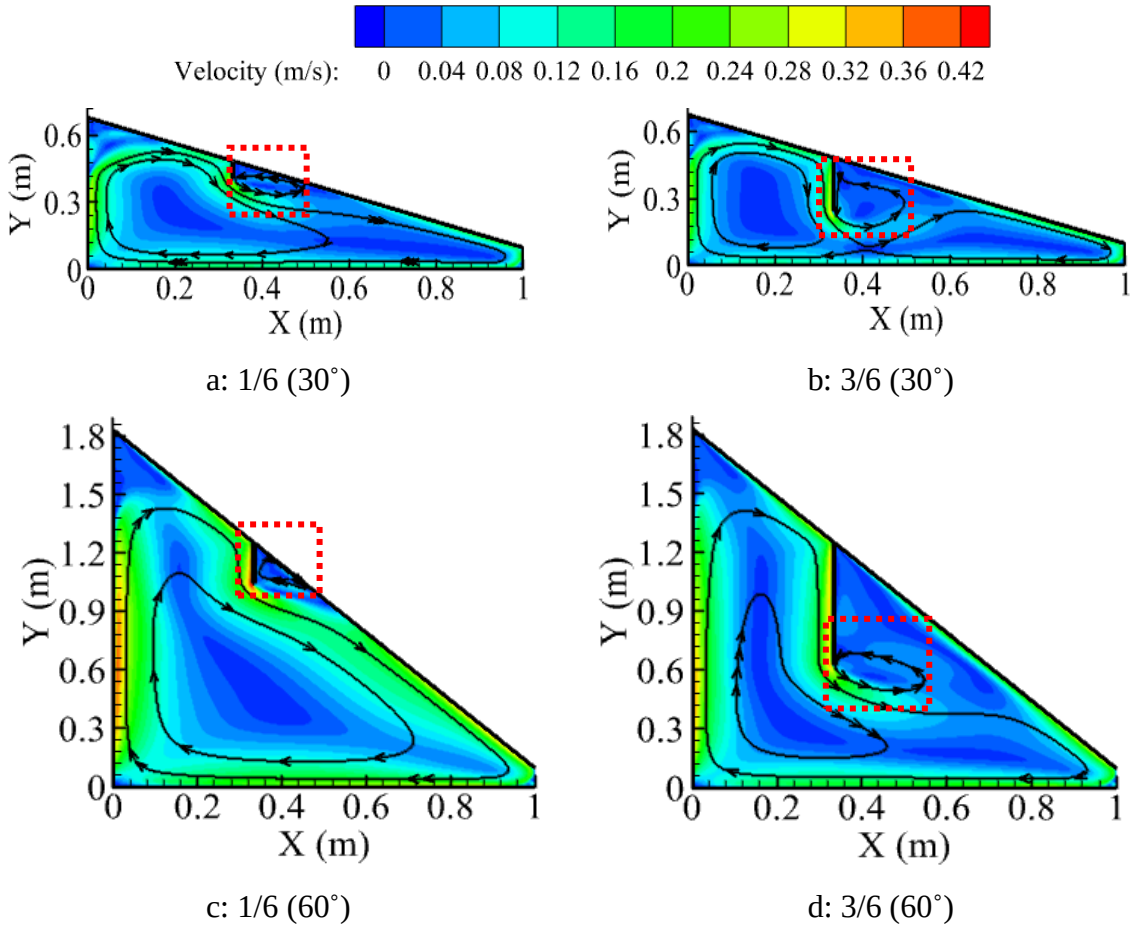

Figure 10: Velocity contours for 30˚ and 60˚ cover angles.

Now, it is interesting to observe that contrary to the shorter baffle lengths, the 5/6 baffle experiences an increase in the heat transfer coefficient for cover angles above 10˚. This implies that the longer baffle (5/6) is more efficient at partitioning the flow, particularly for the 20˚ and 30˚ cover angle geometries. However, at a 40˚ cover angle, the heat transfer coefficient decreases, this is due to the increasing strength of the cell located on the right side of the baffle supressing the flow on left side and delivering two vertical cells as seen in Figure. This same flow pattern is observed at 50˚ and 60˚ and leads to the heat transfer coefficient falling below that of the case without a baffle.

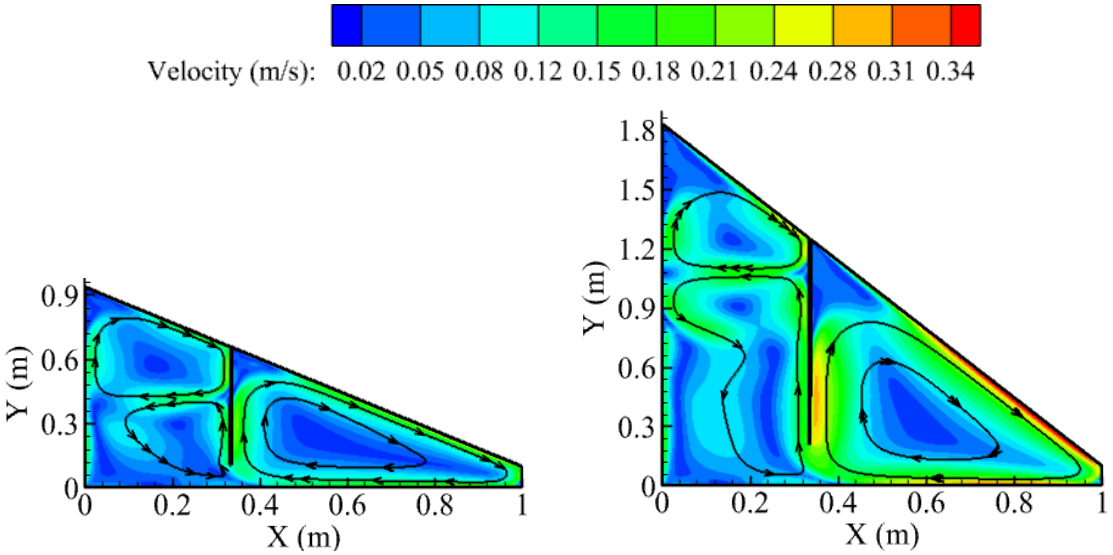

a: 5/6 (40˚) b: 5/6 (60˚)

Figure 11: Velocity contours for 40˚ and 60˚ cover angles.

Evidently, the results show that a baffle mounted near the rear wall of the still does not increase the heat transfer coefficient in all cases. Rather, it appears that it is more effective to use a baffle to enhance heat transfer at lower angles as this aids the development of a favourable multi-cellular flow pattern.

4.2 Baffle mounted mid-width of the still

If the baffle is moved to the middle of the still, it is again seen that the length has an effect on the heat transfer coefficient, and that this varies with cover angle, Figure 12.

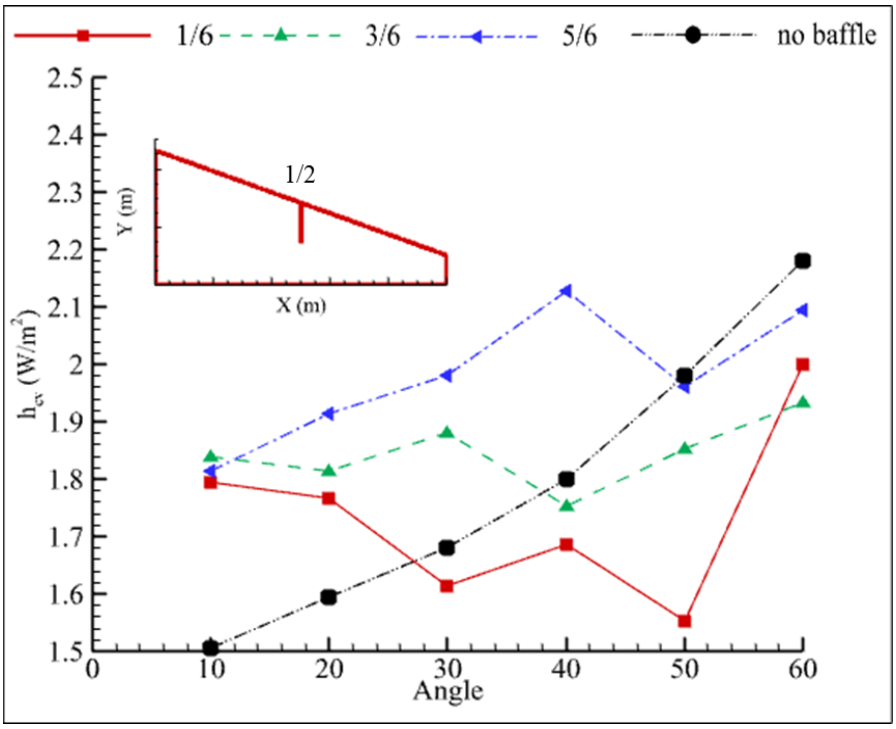

Figure 12: The effect of baffle length and cover angle on the heat transfer coefficient, with the baffle mounted mid-width

As seen previously, the shorter baffle lengths initially aid the development of a multi-cellular flow (Figure 13), which leads to an increase in the heat transfer coefficient. As the cover angle increases however, this multicellular flow begins to break down, leading to the development of a vertical cell arrangement which hinders the transport of heat from the bottom of the enclosure. This flow pattern was observed previously, but is most clearly illustrated in Figure 14, which corresponds to the minimum heat transfer coefficient observed in an enclosure with a baffle mounted mid-width. Moreover, in Figure 15 for a baffle length of 3/6, it is apparent that there is a transition from two vertical cells in the right side of the still to a mono-cellular arrangement, and this corresponds to the changes in the heat transfer coefficient seen in Figure 12.

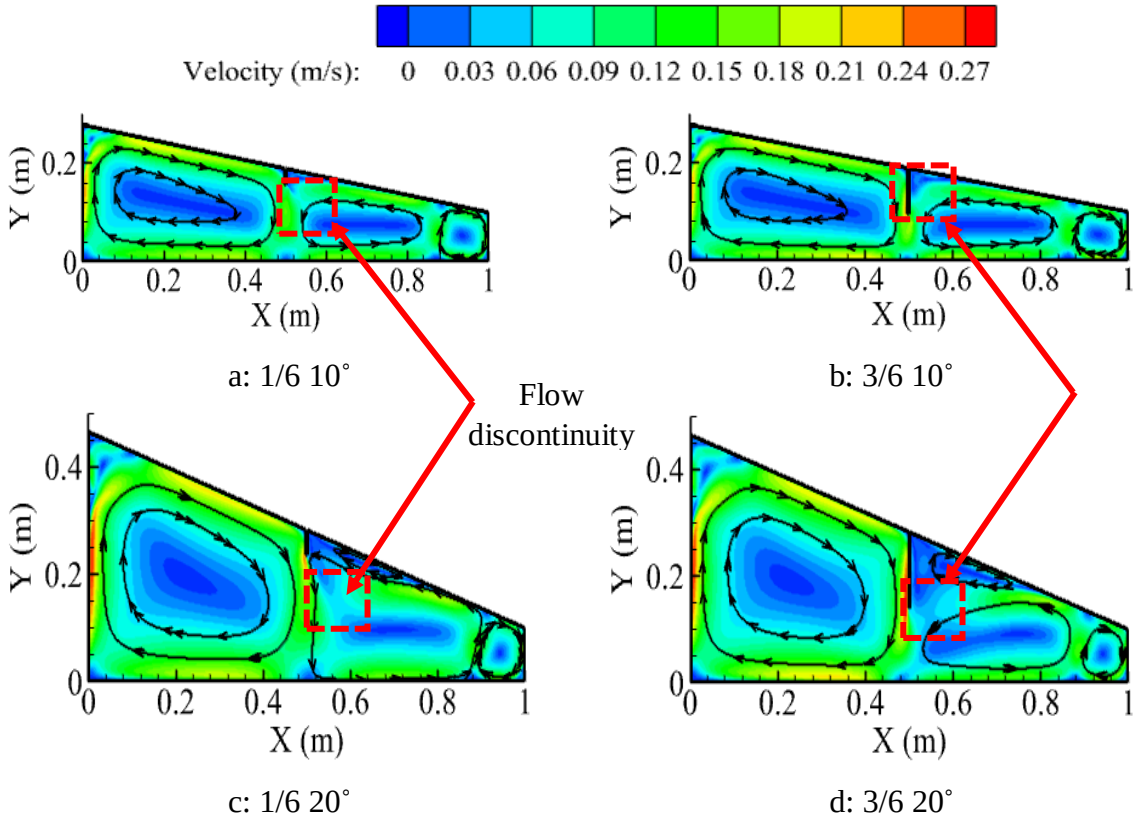

Figure 13: Velocity contours at 10˚ and 20˚ cover angles.

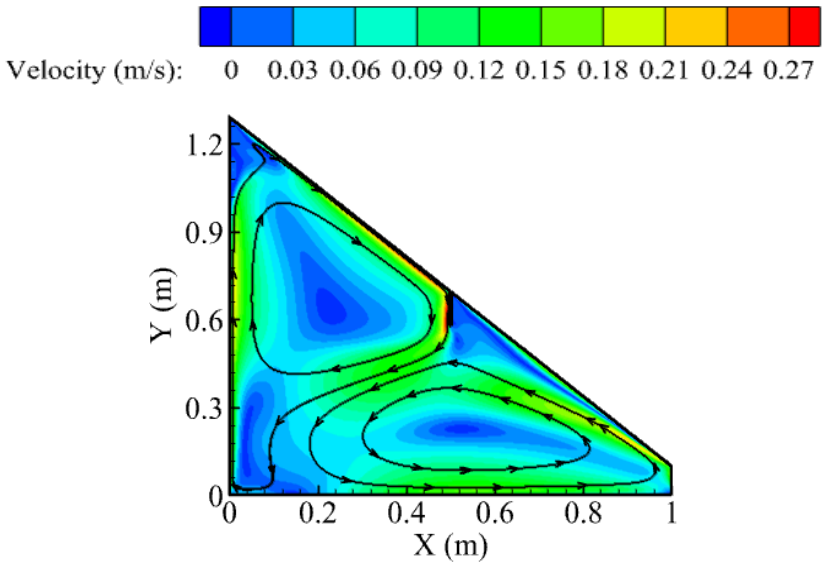

Figure 14: Velocity contours at 50˚ cover angle (1/6 baffle).

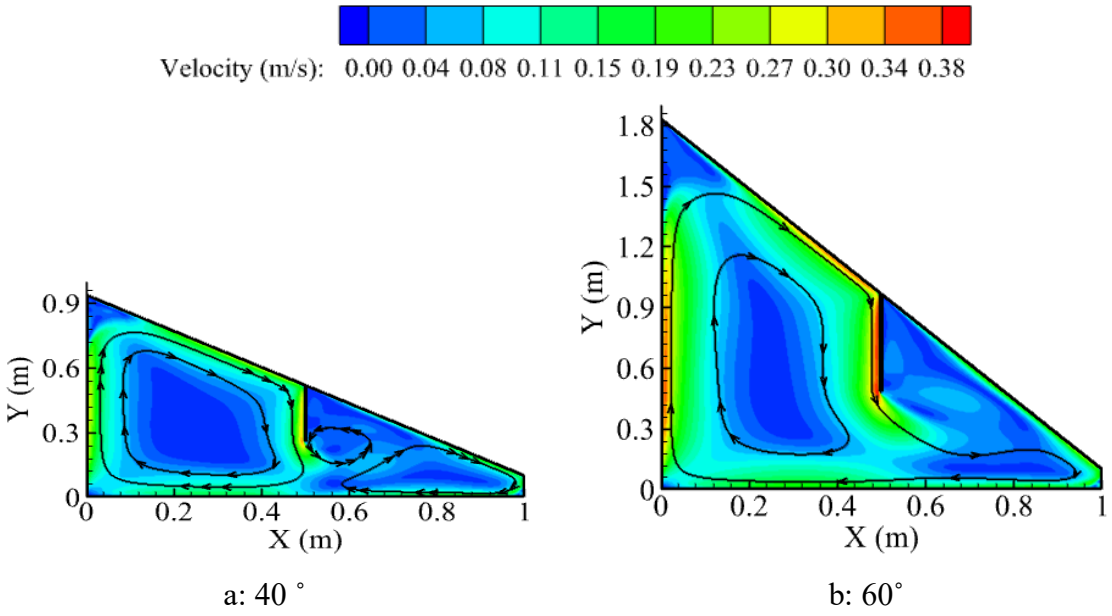

457 Figure 15: Velocity contours for a 3/6 baffle at a: 40°, b: 60° cover angles

458 As with the baffle mounted near the rear wall of the still, it is clear that a mid-position baffle
459 can enhance the natural convection particularly at lower cover angles. However, what is clear
460 is the need to avoid the development of vertical multi-cellular flows which suppress the
461 transport mechanism.

462 **4.3 Baffle mounted near the still's front wall**

463 In the final case, the baffle was positioned at 2/3 of the still's width, close to the front wall. The
464 effect of this on the heat transfer is shown in Figure. Now it is interesting to note that unlike
465 the two preceding baffle locations, in this case the 1/6 baffle has the highest heat transfer
466 coefficient at a 10° cover angle. The reason for this difference in heat transfer coefficient is due
467 to the number of cells generated by the inclusion of the baffle, as seen in Figure. At 1/6 baffle
468 length four cells are observed compared to 3/6 with three cells and 5/6 with 2 cells.
469 Consequently, upward flow of the cells carries heat more efficiently despite the higher velocity
470 flows observed in the other cases.

471 However, following the established pattern, the effect of the 1/6 baffle gradually decreases to
472 reach its lowest value at 40°, lower than no baffle geometry. This is due to the length of the
473 baffle not allowing the creation of the multicellular flow and acting as a barrier, destroying the
474 downward flow adjacent to the top surface.

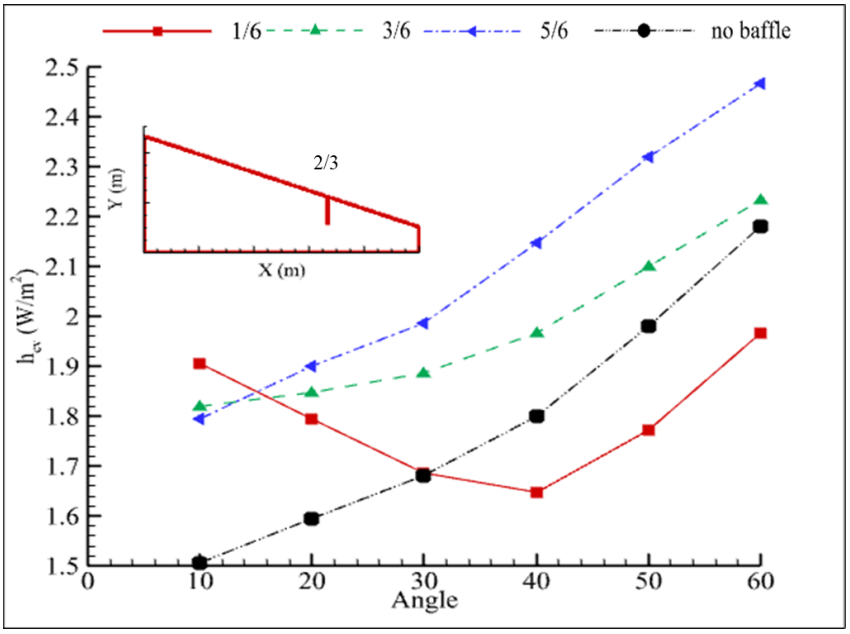

475

476 Figure 16: The effect of baffle length and cover angle on the heat transfer coefficient, with the baffle
477 mounted near the front wall

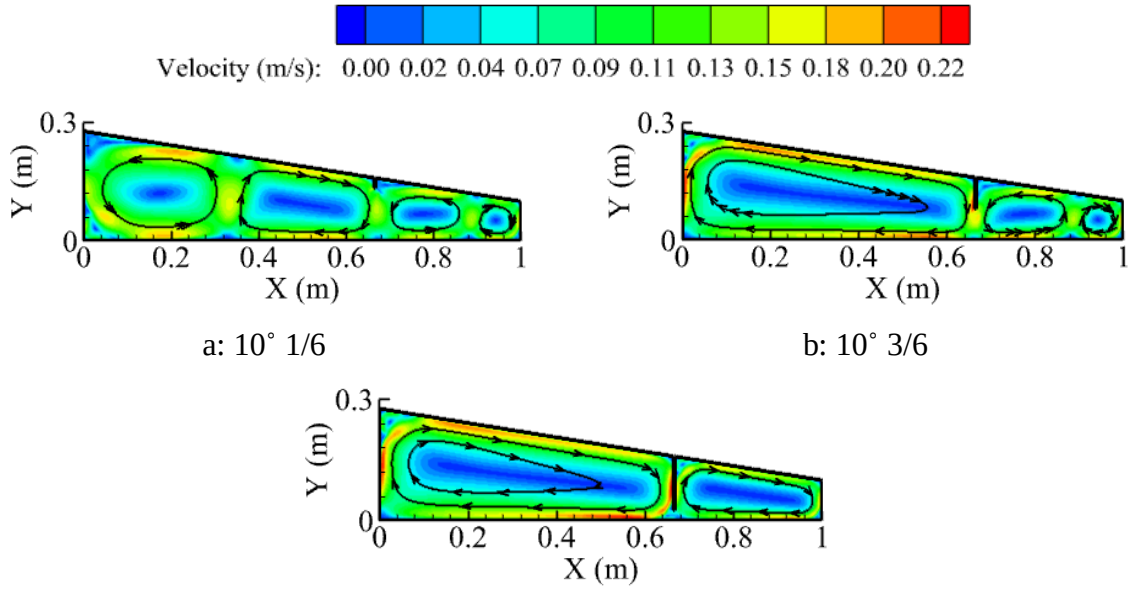

a: 10˚ 1/6

b: 10˚ 3/6

c: 10˚ 5/6

478 Figure 17: Right baffle at a 10˚ cover angle.

479 Interestingly, for both 3/6 and 5/6 baffle lengths the heat transfer coefficient increases with
480 increasing cover angles. This is because the flow for both geometries at this stage is maintained
481 in two cells, as shown in Figure 18. It is worth noting, that this did not occur with baffles
482 positioned to the rear or middle of the still, which moved to a vertical cell arrangement and
483 resulted in a suppression of convection.

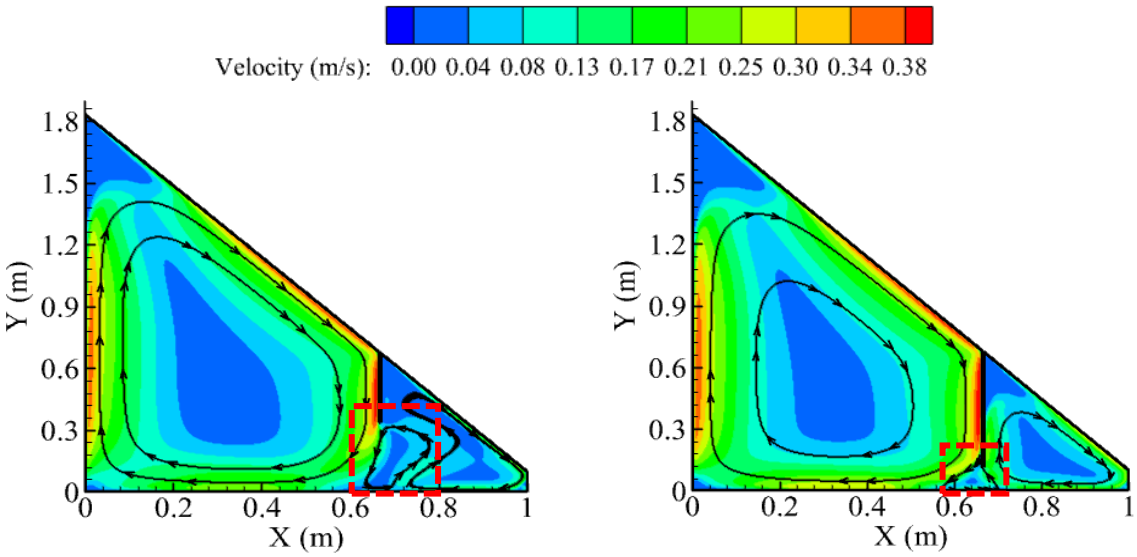

a= 3/6 b= 5/6

Figure 18: Velocity contours at 60˚ cover angle

As such, there appears to be some advantages in mounting baffles close to the front wall as a means of enhancing the convection in solar stills for a wide range of conditions.

4.4 Correlating geometry to heat and mass transfer

As discussed in the above sections, the position of the baffle, its length and the solar still geometry directly affect the magnitude of heat transfer coefficient from the bottom surface, and this is associated with the flow field in the still. With the intention of enhancing the parametric modelling of single slope solar stills, it was decided to establish a correlation describing the heat transfer coefficient as a function of the baffled still geometry.

By generalizing the findings acquired from the CFD modelling, a relation between Nusselt number and the parameters affecting heat transfer inside the cavity can be described by Equation 5:

$$Nu = {Ra_a}^{0.188} * AR^{-0.29} * (\cos\theta)^{-0.5} * \left(\frac{b}{B}\right)^{0.08} * \left(\frac{d}{D}\right)^{0.09} \quad (5)$$

Where: $2.24\times10^7 < Ra_a < 3.03\times10^9$; $10^o < \theta < 60$; $1.04<AR<5.3$; $0.33<b<0.66$; $0.26<d<1.05$

As shown in Figure, the Nusselt number correlation is in good agreement with the numerical, data lying between +15% and -15% of the simulated data. This implies that it should be suitable

to predict heat transfer coefficient for a wide range of cover angles, enclosure aspect ratios and baffle positions and lengths.

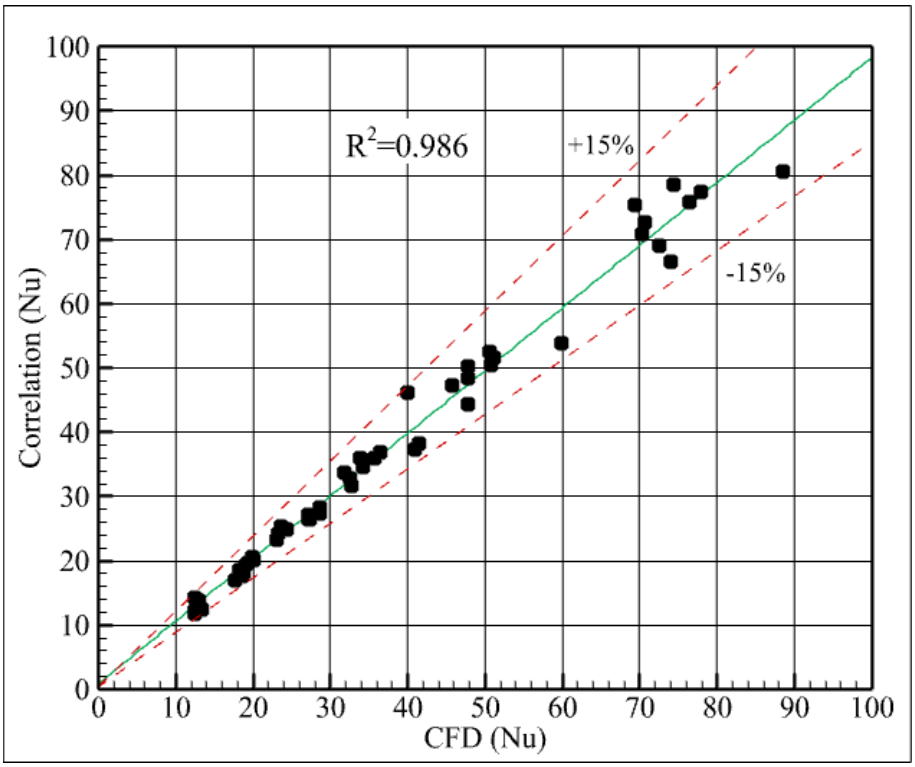

Figure 19: Correlated data of the study

However, in this study only a heat transfer relation as a function of geometry was investigated. In the normal working conditions of solar stills, when enough heat is provided to the water basin, convective and evaporative heat transfer occur simultaneously between the water layer and cover surface. In this respect, to consider the mass transfer in a solar still, Boelter and Sharpley (1938) investigated the relation between evaporative and convective heat transfer from a free water surface. The results of their study showed that for convection alone Rayleigh number varies with $(T_h - T_c)$, and for isothermal evaporation varies with $\left(\frac{M_c T_c}{M_h T_h} - 1\right)$.

Therefore, to adapt Equation 5 to solar still working conditions, the previous correlation should utilise a modified form of the Rayleigh number, as shown in Equation 6.

$$Nu' = {Ra'_a}^{0.188} * AR^{-0.29} * (\cos\theta)^{-0.5} * \left(\frac{b}{B}\right)^{0.08} * \left(\frac{d}{D}\right)^{0.09} \quad (6)$$

Where:

$$Ra'_a = \frac{{\rho_a}^2 \, g \, \beta_a \, \Delta T' \, Cp_a \, L^3}{\lambda_a \mu_a}$$

And this in turn can be used to quantify the evaporative heat transfer, which relates directly to the solar still yield, through an abridged form of Chilton-Colburn analogy as shown in Equation 7 (Sharshir et al, 2020, Abdullah et al, 2020, Cheng et al, 2019, Abdullah et al, 2019).

$$h_{ew} = \left[\frac{\lambda_w}{Cp_a}\frac{M_h}{M_c}\frac{1}{P_T}\right] h_{cv} \quad (7)$$

5. Conclusion

In this study a comprehensive examination was undertaken to examine the effect of baffle position and length on the natural convection inside single slope solar still geometries with a wide range of cover angles and aspect ratios.

The findings indicate that the existence of a baffle in a still had a pronounced effect on the natural convection, and in some cases the baffle increased the convective heat transfer coefficient, a proxy for the still's yield, by almost 20%. However, the position and length of the baffle need careful consideration to establish the appropriate flow and avoid a decrease in the heat transfer coefficient.

It was found that short baffles had the greatest impact at lower cover angles, for all baffle locations. In addition, it was shown that baffles mounted closer to the front wall offered enhanced heat transfer over a broader range of conditions. Furthermore, geometries leading to multiple vertical cells need to be avoided, as these result in suppression of the natural convection transport mechanism. Moreover, careful attention needs to be given to the material of the baffle, high transmittance materials with low conductivity are most suitable, as these avoid heat transfer through the baffle and shading of the absorber. Finally, a correlation was developed to describe the natural convection in baffled solar stills, that it is hoped will aid designers of these systems in the future.

Acknowledgement

The authors thank the Ministry of Foreign Affairs and Trade, New Zealand for the financial support provided to conduct this research.

References

Abdallah, S., Abu-Khader, M.M. and Badran, O., 2009. Effect of various absorbing materials on the thermal performance of solar stills. Desalination, 242(1): 128-137.

Abdullah, A.S., Essa, F.A., Omara, Z.M., Rashid, Y., Hadj-Taieb, L., Abdelaziz, G.B. and Kabeel, A.E., 2019. Rotating-drum solar still with enhanced evaporation and condensation techniques: Comprehensive study. Energy Conversion and Management, 199: 112024.

Abdullah, A.S., Younes, M.M., Omara, A.M. and Essa, F.A., 2020. New design of trays solar still with enhanced evaporation methods – Comprehensive study. Solar Energy, 203: 164-174.

Acharya, F.M.S., 2000. Natural convection in trapezoidal cavities with baffles mounted on the upper inclined surfaces. Numerical Heat Transfer, Part A: Applications, 37(6): 545-565.

Al-Hamadani, A.A. and Shukla, S. 2013. Performance of single slope solar still with solar protected condenser. Distributed Generation and Alternative Energy Journal, 28(2): 6-28.

Alipanah, F. and Rahbar, N. 2018. CFD simulation and second law analysis of weir-type cascade solar stills with different number and dimensions of steps. Desalin. Water Treat., 104: 15-27.

Altaç, Z. and Uğurlubilek, N. 2016. Assessment of turbulence models in natural convection from two- and three-dimensional rectangular enclosures. International Journal of Thermal Sciences, 107: 237-246.

Anderson, T.N., Duke, M. and Carson, J.K., 2010, Experimental determination of natural convection heat transfer coefficients in an attic shaped enclosure. International Communications in Heat and Mass Transfer, 37(4): 360-363

ANSYS Inc., 2015. FLUENT user's guide, Ansys, Canonsburg.

Arunkumar, T., Kabeel, A.E., Raj, K., Denkenberger, D., Sathyamurthy, R., Ragupathy, P. and Velraj, R., 2018. Productivity enhancement of solar still by using porous absorber with bubble-wrap insulation. Journal of Cleaner Production, 195: 1149-1161.

567 Asan, H. and Namli, L. 2001. Numerical simulation of buoyant flow in a roof of triangular
568 cross-section under winter day boundary conditions. Energy and Buildings, 33(7): 753-757.

569 Azooz, A. and Younis, G. 2016. Effect of glass inclination angle on solar still performance.
570 Journal of Renewable and Sustainable Energy, 8(3): 033702.

571 Cheng, W.-L., Huo, Y.-K. and Nian, Y.-L. 2019. Performance of solar still using shape-
572 stabilized PCM: Experimental and theoretical investigation. Desalination, 455: 89-99.

573 Cherraye, R., Bouchekima, B., Bechki, D., Bouguettaia, H. and Khechekhouche, A., 2020,
574 The effect of tilt angle on solar still productivity at different seasons in arid conditions (south
575 Algeria). International Journal of Ambient Energy,
576 https://doi.org/10.1080/01430750.2020.1723689

577 Dev, R. and Tiwari, G.N. 2009. Characteristic equation of a passive solar still. Desalination,
578 245(1): 246-265.

579 Djebedjian, B., and Abou Rayan, M. (2000). Theoretical investigation on the performance
580 prediction of solar still. Desalination, 128(2), 139-145.

581 Dwivedi, V. K., and Tiwari, G. N. (2009). Comparison of internal heat transfer coefficients in
582 passive solar stills by different thermal models: an experimental
583 validation. Desalination, 246(1-3), 304-318.

584 El-Sebaii, A.A. and M. El-Naggar, 2017. Year round performance and cost analysis of a
585 finned single basin solar still. Applied Thermal Engineering, 110: 787-794.

586 El-Sebaii, A.A., Ramadan, M.R.I, Aboul-Enein, S. and El-Naggar, M. 2015. Effect of fin
587 configuration parameters on single basin solar still performance. Desalination, 365: 15-24.

588 El-Sebaii, A.A., Aboul-Enein, S. and El-Bialy, E. 2000. Single basin solar still with baffle
589 suspended absorber. Energy Conversion and Management, 41(7): 661-675.

590 Feilizadeh, M., Soltanieh, M., Karimi Estahbanati, M.R., Jafarur, K., and Ashrafmansouri, S.
591 2017. Optimization of geometrical dimensions of single-slope basin-type solar stills.
592 Desalination, 424: 159-168.

Flack, R.D., 1980. The experimental measurement of natural convection heat transfer in triangular enclosures heated or cooled from below. Journal of Heat Transfer, 102(4): 770-772.

Gaur, M. K., and Tiwari, G. N., 2010. Optimization of number of collectors for integrated PV/T hybrid active solar still. Applied Energy, 87(5), 1763-1772.

Gude, V.G., 2017. Desalination and water reuse to address global water scarcity. Reviews in Environmental Science and Bio/Technology, 16(4): 591-609.

Hák, T., Janoušková, S. and Moldan, B. 2016. Sustainable Development Goals: A need for relevant indicators. Ecological Indicators, 60: 565-573.

Hassan, H., Yousef, M.S., Fathy, M. and Salem Ahmed, M., 2020. Impact of condenser heat transfer on energy and exergy performance of active single slope solar still under hot climate conditions. Solar Energy, 204: 79-89.

Jamil, B. and Akhtar, N. 2017, Effect of specific height on the performance of a single slope solar still: An experimental study. Desalination, 414: 73-88.

Karimi Estahbanati, M.R., Ahsan, A., Feilizadeh, M., Jafarpur, K. Ashrafmansouri, S. and Feilizadeh, M., 2016. Theoretical and experimental investigation on internal reflectors in a single-slope solar still. Applied Energy, 165: 537-547.

Keshtkar, M., Eslami, M. and Jafarpur, K., 2020. Effect of design parameters on performance of passive basin solar stills considering instantaneous ambient conditions: A transient CFD modeling. Solar Energy, 201: 884-907.

Kumar, S., and Tiwari, G. N., 2009. Thermal modelling, validation and exergetic analysis of a hybrid Photovoltaic/Thermal (PV/T) active solar still. International Journal of Exergy, 6(4), 567-591.

Kumar, S., and Tiwari, G. N. (1996). Estimation of convective mass transfer in solar distillation systems. Solar energy, 57(6), 459-464.

618 Kumar, S., Tiwari, G. N., and Gaur, M. K., 2010. Development of empirical relation to
619 evaluate the heat transfer coefficients and fractional energy in basin type hybrid (PV/T)
620 active solar still. Desalination, 250(1), 214-221.

621 Lartigue, B., Lorente, S., and Bourret, B., 2000. Multicellular natural convection in a high
622 aspect ratio cavity: experimental and numerical results. International journal of heat and mass
623 transfer, 43(17), 3157-3170.

624 Madiouli, J., Lashin, A., Shigidi, I., Badruddin, I. A., and Kessentini, A., 2020. Experimental
625 study and evaluation of single slope solar still combined with flat plate collector, parabolic
626 trough and packed bed. Solar Energy, 196, 358-366.

627 Omri, A., Orfi, J., and Nasrallah, S. B. (2005). Natural convection effects in solar
628 stills. Desalination, 183(1-3), 173-178.

629 Panchal, H., Patel, P., Patel, N. And Thakkar, H. 2017. Performance analysis of solar still
630 with different energy-absorbing materials. International Journal of Ambient Energy, 38(3):
631 224-228.

632 Panchal, H.N. and Patel, S., 2017. An extensive review on different design and climatic
633 parameters to increase distillate output of solar still. Renewable and Sustainable Energy
634 Reviews, 69: 750-758.

635 Panchal, H.N. and Patel, N., 2018. ANSYS CFD and experimental comparison of various
636 parameters of a solar still. International Journal of Ambient Energy, 39(6): 551-557.

637 Parsa, S. M., Rahbar, A., Javadi, D., Koleini, M. H., Afrand, M., and Amidpour, M., 2020.
638 Energy-matrices, exergy, economic, environmental, exergoeconomic, enviroeconomic, and
639 heat transfer (6E/HT) analysis of two passive/active solar still water desalination nearly
640 4000m: Altitude concept. Journal of Cleaner Production, 261, 121243.

641 Poulikakos, D. and Bejan, A. 1983. Natural convection experiments in a triangular enclosure.
642 J. Heat Transfer, 105(3): 652-655

643 Raffel, M., Willert, C.E., Wereley, S. and Kompenhans, J., 2018, Particle image velocimetry:
644 a practical guide. Springer, Berlin

645 Rahbar, N., and Esfahani, J. A. (2012). Estimation of convective heat transfer coefficient in a
646 single-slope solar still: a numerical study. Desalination and water treatment, 50(1-3), 387-
647 396.

648 Rashidi, S., Esfahani, J.A. and Rahbar, N., 2017. Partitioning of solar still for performance
649 recovery: Experimental and numerical investigations with cost analysis. Solar Energy, 153:
650 41-50.

651 Rashidi, S., Bovand, M. and Esfahani, J.A., 2016. Optimization of partitioning inside a single
652 slope solar still for performance improvement. Desalination, 395: 79-91.

653 Rashidi, S., Bovand, M., Rahbar, N. and Esfahani, J.A., 2018. Steps optimization and
654 productivity enhancement in a nanofluid cascade solar still. Renewable Energy, 118: 536-
655 545.

656 Rheinländer, J. (1982). Numerical calculation of heat and mass transfer in solar stills. Solar
657 Energy, 28(2), 173-179.

658 Rincón-Casado, A., Sanchez de la Flor, F.J., Chacon Vera, E. and Sanchez Ramos, J., 2017.
659 New natural convection heat transfer correlations in enclosures for building performance
660 simulation. Engineering Applications of Computational Fluid Mechanics, 11(1): 340-356.

661 Sakthivel, T. and Arjunan, T. 2019. Thermodynamic performance comparison of single slope
662 solar stills with and without cotton cloth energy storage medium. Journal of Thermal
663 Analysis and Calorimetry, 137(1): 351-360.

664 Sharpley, B.F. and Boelter, L.M.K., 1938. Evaporation of water into quiet air from a one-foot
665 diameter surface. Industrial and Engineering Chemistry, 30(10): 1125-1131.

666 Sharshir, S.W., Yang, N., Peng, G. and Kabeel, A.E. 2016. Factors affecting solar stills
667 productivity and improvement techniques: A detailed review. Applied Thermal Engineering,
668 100: 267-284.

669 Sharshir, S.W., Eltawil, M.A., Algazzar, A.M. Sathyamurthy, R. and Kandeal, A.W. 2020.,
670 Performance enhancement of stepped double slope solar still by using nanoparticles and linen
671 wicks: Energy, exergy and economic analysis. Applied Thermal Engineering, 174: 115278.

672 Siva Sankaran, N. and Sridharan, M. 2020, Experimental research and performance study of
673 double slope single basin solar distillation still using CFD techniques. International Journal of
674 Ambient Energy, https://doi.org/10.1080/01430750.2020.1852109

675 Srivastava, P.K. and Agrawal, S.K., 2013. Winter and summer performance of single sloped
676 basin type solar still integrated with extended porous fins. Desalination, 319: 73-78.

677 Subhani, S. and Kumar, R.S. 2019. Numerical investigation on influence of mounting baffles
678 in solar stills. in AIP Conference Proceedings. AIP Publishing LLC.
679 https://doi.org/10.1063/1.5127616

680 Tanaka, H., 2009. Experimental study of a basin type solar still with internal and external
681 reflectors in winter. Desalination, 249(1): 130-134.

682 Tiwari, A. K., and Tiwari, G. N. (2005). Effect of the condensing cover's slope on internal
683 heat and mass transfer in distillation: an indoor simulation. Desalination, 180(1-3), 73-88.

684 Tiwari, G. N., Mishra, A. K., Meraj, M., Ahmad, A., and Khan, M. E., 2020. Effect of shape
685 of condensing cover on energy and exergy analysis of a PVT-CPC active solar distillation
686 system. Solar Energy, 205, 113-125.

687 Varol, Y., Oztop, H.F. and Varol, A., 2007. Effects of thin fin on natural convection in
688 porous triangular enclosures. International Journal of Thermal Sciences, 46(10): 1033-1045.

689 Velmurugan, V., Deenadalayan, C.K., Vinod, H. and Srithar, K., 2008. Desalination of
690 effluent using fin type solar still. Energy, 33(11): 1719-1727.

691 Wu, Q., Zhu, C. A., Liu, L., Liu, J., and Luo, Z., 2019. Two-dimensional flow visualization
692 and velocity measurement in natural convection near indoor heated surfaces using a thermal
693 image velocimetry method. Applied Thermal Engineering, 146, 556-568.

694 Yousef, M.S. and Hassan, H. 2019. An experimental work on the performance of single slope
695 solar still incorporated with latent heat storage system in hot climate conditions. Journal of
696 Cleaner Production, 209: 1396-1410.